

Probing the CP nature of Higgs boson through $e^-e^+ \rightarrow e^-e^+\phi$

Qing-Hong Cao*

Physics Department, University of California at Riverside, Riverside, CA 92521, USA

F. Larios†

*Departamento de Física Aplicada, CINVESTAV-Mérida,
AP 73 Cordemex, 97310 Mérida, Yucatán, Mexico*

G. Tavares-Velasco‡

*Facultad de Ciencias Físico Matemáticas,
Benemérita Universidad Autónoma de Puebla,
Apartado Postal 1152, Puebla, Pue., México*

C.-P. Yuan§

*Department of Physics & Astronomy,
Michigan State University, East Lansing, Michigan 48824, USA*

Abstract

We study the production of Higgs boson (ϕ) via the $e^-e^+ \rightarrow e^-e^+\phi$ process at a future International Linear Collider (ILC) with $\sqrt{S} = 1$ TeV. At this energy the ZZ -fusion rate, as predicted by the Standard Model, dominates over the associated ZH production rate. Here, we consider a class of theory models based on the effective ϕVV (with $V = Z, \gamma$) couplings generated by dimension-6 operators. We also show how to use the kinematical distributions of the final state leptons to discriminate the CP-even and CP-odd Higgs bosons produced at the ILC, when the $\phi\gamma\gamma$ coupling dominates the Higgs boson production rate.

PACS numbers: 11.30.Er, 13.66.Hk, 14.80.Cp

*Electronic address: qcao@ucr.edu

†Electronic address: larios@mda.cinvestav.mx

‡Electronic address: gtv@cfm.buap.mx

§Electronic address: yuan@pa.msu.edu

I. INTRODUCTION

Currently the only missing piece of the Standard Model (SM) is the Higgs boson, which plays a vital role in this theory as it is assumed to be responsible for the mechanism of electroweak symmetry breaking (EWSB). Although only a single neutral CP-even Higgs boson is present in the SM, more than one Higgs boson may exist in several new physics models. For example, the two-Higgs doublet model (THDM), one of the simplest extensions of the SM, predicts the existence of three neutral and two charged Higgs bosons. In the CP-conserving THDM, two of the neutral Higgs bosons are CP-even and the remaining one is CP-odd. If CP violation appears in the scalar potential, the three neutral Higgs bosons may be a mixture of the CP eigenstates.

The hopes to observe a Higgs boson at the CERN LEP collider faded away. The lower bound on the SM Higgs boson (H) mass $m_H \geq 115$ GeV was obtained from studying the process $e^-e^+ \rightarrow ZH$ after combining the data taken by the four LEP experiments. The main Higgs boson production mechanism for a Higgs boson with mass around a few hundred GeV at a hadron collider, such as the Fermilab Tevatron and the CERN Large Hadron Collider (LHC), is through gluon fusion process. For $m_H \leq 2m_W$, the Higgs boson will decay predominantly into a $b\bar{b}$ pair, but detecting Higgs boson via this channel is challenging because of the large QCD backgrounds. In this mass range the rare decay modes $H \rightarrow \gamma\gamma$ and $H \rightarrow WW^*, ZZ^*$ are the most promising channels for detecting a SM Higgs boson. With enough integrated luminosity, the Tevatron Run-II is expected to offer the possibility of finding a Higgs boson with a mass up to 130 GeV through the associated WH or ZH production processes. At the LHC, the gluon fusion production mechanism will allow us to search for a Higgs boson via the $H \rightarrow \gamma\gamma$ decay mode for m_H lower than about 130 GeV, whereas for m_H ranging from 130 GeV to 180 GeV the $H \rightarrow WW^*, ZZ^*$ decay modes could yield an observable signal [1].

Once a Higgs boson is detected, the next task will be to find out whether it is the SM Higgs boson or some other scalar bosons predicted by other theories. To this aim it is crucial to determine the properties of this particle, which may shed light on the EWSB mechanism. Therefore, apart from a precise determination of the Higgs boson mass (or masses if there is more than one Higgs boson), one of the main tasks of future colliders will be to determine

other properties of Higgs boson, such as its decay rates, its couplings to other particles, its properties of transformation under the discrete symmetries C (charge conjugation) and P (parity). Several methods have been proposed in the literature to determine the CP properties of a Higgs boson at hadron [2, 3, 4, 5, 6, 7], lepton [8, 9, 10, 11, 12, 13, 14, 15, 16, 17, 18, 19, 20, 21] and photon [22, 23, 24, 25] colliders. Some of these methods rely on the study of certain energy and angular correlations of the decay products of the Higgs boson, whereas others concentrate on the change in its production rate due to the structure of its couplings to gauge bosons or heavy fermions. For instance, it was shown that polarized photon beams could be used to determine the CP property of a Higgs boson produced at resonance via photon fusion process [22]. Also, the spin and parity properties of the Higgs boson were analyzed for the $e^-e^+ \rightarrow ZH$ process [8]. In this work we show that the $e^-e^+ \rightarrow e^-e^+\phi$ process through VV (with $V = Z, \gamma$) fusion at the future International Linear Collider (ILC) could help us to determine the CP nature of the Higgs boson. It has long been known that for large center-of-mass energies (greater than about 500 GeV) the ZZ fusion channel becomes dominant in the $e^-e^+ \rightarrow e^-e^+\phi$ process [26]. In Ref. [21], it was shown how to measure the degree of CP violation in the Higgs sector via ZZ fusion process at a $\sqrt{S} = 500$ GeV ILC. As a complementary study, we will not consider CP violating cases in this work. We shall assume CP invariant interactions and study how to determine the CP property of the Higgs boson produced at the ILC with a higher center-of-mass energy ($\sqrt{S} = 1$ TeV). Since at this energy, ZZ fusion contributes with 95% of the total cross section, as predicted by the SM, we choose to focus on the VV fusion channel alone.

Rather than focusing on some specific model and calculating the respective loop contributions to the ϕVV vertex, our study is based on the general Lorentz invariant scalar-vector boson vertex. In general, three possible couplings ϕZZ , $\phi Z\gamma$ and $\phi\gamma\gamma$, may give rise to ZZ , $Z\gamma$ and $\gamma\gamma$ fusion processes, which at high energies will become the main source of Higgs boson production. As we shall see later, we found that the effects of the $\phi\gamma\gamma$ couplings are more effective for our task, as they can give large contributions to $e^-e^+\phi$ production due to collinear enhancement.

The rest of this work is organized as follows. In Section II we present a brief description of the general couplings. Section III is devoted to a Monte Carlo analysis for the $e^-e^+ \rightarrow e^-e^+\phi$ process. Both polarized and unpolarized beams are considered and special attention is paid

to those kinematical distributions which are sensitive to both the strength of the anomalous ϕVV coupling and the CP property of the Higgs boson. Our conclusions will be presented in Section IV. Finally, the helicity amplitudes for the $e^-e^+ \rightarrow e^-e^+\phi$ process are presented in Appendix A for completeness.

II. ANOMALOUS ϕVV COUPLING

The general Higgs-gauge boson vertex describing $\phi\gamma\gamma$, $\phi Z\gamma$ and ϕZZ couplings can be written as:

$$\Gamma_{\phi VV}^{\mu\nu} = i a_{\phi ZZ} g^{\mu\nu} + i \frac{g_{\phi VV}}{v} (p_2^\mu p_1^\nu - g^{\mu\nu} p_1 \cdot p_2) + i \frac{\tilde{g}_{\phi VV}}{v} \varepsilon^{\mu\nu\rho\sigma} p_{1\rho} p_{2\sigma}, \quad (1)$$

where p_1^μ and p_2^ν are the momenta of the gauge bosons. The $a_{\phi ZZ} g^{\mu\nu}$ term represents the dimension-4 coupling that appears in models such as the SM, the THDM and the MSSM. For simplicity, we will use the SM value $a_{\phi ZZ} = 2 M_Z^2/v$ in our study.

The anomalous ϕVV (with $V = \gamma, V$) couplings with dimension more than four could arise at the one-loop level in a renormalizable theory. Also, from the standpoint of the effective Lagrangian approach (ELA) [27, 28], these couplings can be induced by dimension 6 (and higher) operators [29, 30]. For example, an effective Lagrangian using a $SU(2) \times U(1)$ scalar doublet that couples with the gauge bosons through dimension-6 operators would be:

$$\mathcal{L}_{eff}^{\phi VV} = \frac{1}{\Lambda^2} \sum_i \left(f_i \mathcal{O}_i + \tilde{f}_i \tilde{\mathcal{O}}_i \right), \quad (2)$$

where the CP-conserving operators \mathcal{O}_i are given by [31]

$$\mathcal{O}_{BW} = \Phi^\dagger B_{\mu\nu} W^{\mu\nu} \Phi,$$

$$\mathcal{O}_{WW} = \Phi^\dagger W_{\mu\nu} W^{\mu\nu} \Phi,$$

$$\mathcal{O}_{BB} = \Phi^\dagger B_{\mu\nu} B^{\mu\nu} \Phi,$$

in which Φ is the Higgs doublet, $B_{\mu\nu} = ig' B_{\mu\nu}$ and $W_{\mu\nu} = ig/2 \sigma^a W_{\mu\nu}^a$, with $B_{\mu\nu}$ and $W_{\mu\nu}^a$ the strength tensors of the gauge fields; g' and g are U(1) and SU(2) gauge couplings, respectively. As for the CP-violating operators $\tilde{\mathcal{O}}_i$, they are obtained from the above ones after replacing either of the two strength tensors by their respective dual [23]. The simultaneous presence

of both $g_{\phi VV}$ and $\tilde{g}_{\phi VV}$ for one boson would signal CP violation. As mentioned, we will not consider that case in this work, for this we refer the reader to Ref. [21]. In our study we assume a SM-like CP-even Higgs boson h with anomalous couplings g_{hVV} and/or a CP-odd Higgs boson A of same mass but with couplings \tilde{g}_{AVV} .¹ We will also refer to the SM Higgs boson H for the purpose of comparison. Throughout this paper, we refer the production of the SM Higgs boson H as the one generated from the Born level dimension-4 HZZ coupling. Even though higher dimension anomalous operators may arise from loop corrections, we will assume their effects to be negligible. In contrast, for the production of the SM-like Higgs boson h , we include both the Born level dimension-4 HZZ coupling and the higher dimension anomalous g_{hVV} couplings in our calculations. For the production of the CP-odd Higgs boson A , only the higher dimension anomalous \tilde{g}_{AVV} couplings are included.

A common approach for determining the CP property of Higgs boson is to examine the $Z\phi$ associated production ($e^-e^+ \rightarrow Z\phi \rightarrow f^-f^+\phi$) and analyze the angular distribution of the Z decay products [8]. Evidently, for this approach the relevant coupling is ϕZZ (or $\phi Z\gamma$). In this work we will consider a higher energy of 1 TeV for the e^+e^- collider and examine the $e^-e^+ \rightarrow e^-e^+\phi$ process. At this energy VV fusion ($V = Z, \gamma$) becomes dominant. Eventually, we will focus on the $\gamma\gamma$ fusion sub-process which gives a substantial production rate and could be analyzed to study the CP nature of the Higgs boson ϕ .

In order to make any predictions for those processes involving the effective ϕVV coupling, it is necessary to know the order of magnitude of the effective coupling constants $g_{\phi VV}$. Several processes have been discussed in the literature that can be used to obtain bounds on these coefficients. In particular, based on the ELA, the constraints from the LEP and the Tevatron on the reactions $e^+e^- \rightarrow \gamma\gamma\gamma$, $p\bar{p} \rightarrow jj\gamma\gamma$, $p\bar{p} \rightarrow \gamma\gamma + E_T$, and $p\bar{p} \rightarrow \gamma\gamma\gamma$ are known to yield bounds on f_i/Λ^2 [2, 31]. To be consistent with the bounds reported in Ref. [2] we will consider $|f_i|/\Lambda^2 \leq 50 \text{ TeV}^{-2}$, which implies $|g_{\phi VV}| \leq 0.3$ in our notation, cf. Eq. (1).

¹ In general, the CP-odd Higgs boson can have a mass different from the CP-even Higgs boson. Since the goal of this study is to develop methods for determining the CP property of the Higgs boson, we assume a similar mass for these Higgs bosons to simplify our comparison.

III. MONTE CARLO ANALYSIS FOR $e^-e^+ \rightarrow e^-e^+\phi$

We now turn to discuss how the $e^-e^+ \rightarrow e^-e^+\phi$ process can be used to determine the CP property of the Higgs boson. In the following, H stands for the SM Higgs boson, and as discussed above, h and A denote the CP-even and the CP-odd Higgs boson, respectively.

The Feynman diagrams for $e^-e^+ \rightarrow e^-e^+\phi$ are shown in Fig. 1. For the SM Higgs boson H , the contributions arise from Higgstrahlung (the left diagram) and vector-boson fusion (the right diagram) processes. For the CP-even Higgs boson h , in addition to the SM diagrams there would be contributions arising from the higher dimension hVV couplings. In contrast, for the CP-odd Higgs boson A , the contributions arise only from the higher dimension AVV operators, as there is no SM-like tree level AZZ coupling.

We will carry out a Monte Carlo study and construct some CP-odd observables which are sensitive to the strength of the anomalous ϕVV couplings and can be used to discriminate a CP-even from a CP-odd Higgs boson. In our analysis we will consider both unpolarized and polarized lepton beams, and the convention for the momenta of the external particles is taken as follows

$$e^-(p_1)e^+(p_2) \rightarrow e^-(p_3)e^+(p_4)\phi(p_5), \quad (3)$$

where p_1 and p_2 are the incoming momenta and p_3 , p_4 and p_5 are out-going momenta.

Given the effective interaction of Eq. (1), it is straightforward to calculate the helicity amplitudes for $e^-e^+ \rightarrow e^-e^+\phi$. To this end we used the spinor product formalism introduced in Refs. [32, 33]. The resulting amplitudes are presented in Appendix A for the sake of completeness. To numerically illustrate the method of our analysis, we will take the Higgs boson mass to be 115 GeV (for each $\phi = H, h, A$) and the center-of-mass energy of the e^+e^- collider to be 1 TeV.

We will discuss first the case of unpolarized beams.

A. Initial considerations and basic cuts for the $\gamma\gamma$ fusion t -channel diagram

The $e^-e^+ \rightarrow e^-e^+\phi$ processes can be divided into two sub-processes: the Higgstrahlung process ($V\phi$ production with subsequent decay of the vector boson V into the pair of charged leptons) and the vector-boson fusion process. The Higgstrahlung process is s -channel like

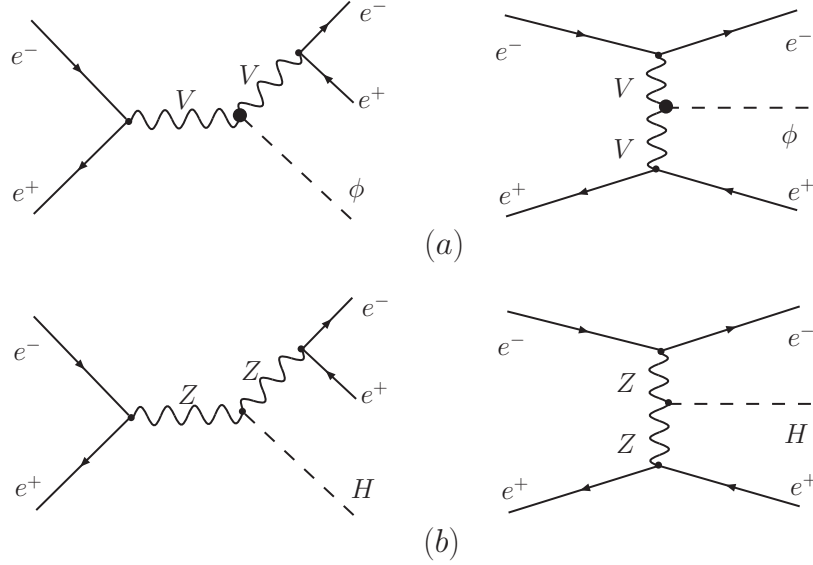


Figure 1: Feynman diagrams for $e^-e^+ \rightarrow e^-e^+\phi$: (a) the effective theory where the heavy dot denotes the effective ϕVV coupling ($V = \gamma, Z$); (b) the Standard Model.

while the vector-boson fusion process is t -channel like. We can separate them by examining the invariant mass of the outgoing e^-e^+ pair. (Of course, for $Z\phi$ production one can include the other decay modes of the Z boson which are not considered in this study). In the Higgstrahlung process, the two final state charged leptons originate from the vector-boson decay. Therefore, if we require the invariant mass ($M_{34} = m_{e^+e^-}$) to be within a 10 GeV range of the Z -boson mass, the cross section will come mostly from the s -channel diagram. Otherwise, the main contribution will come from the t -channel (ZZ fusion) diagram.

On the other hand, both s - and t -channel diagrams may have a singular behavior when the $\phi\gamma\gamma$ (or $\phi Z\gamma$) coupling is considered. In particular, collinear and nearly on-shell photon divergences appear, and we must impose appropriate cuts to avoid these kinematical regions. In this work we will start by imposing the following conditions:

$$\begin{aligned}
 |\cos \theta_3|, |\cos \theta_4| &\leq 0.99, \\
 P_{T3}, P_{T4} &\geq 10 \text{ GeV}, \\
 M_{34} &\geq 5 \text{ GeV}.
 \end{aligned} \tag{4}$$

Here, the angle θ_3 (θ_4) is the polar angle of the outgoing electron (positron). The incoming electron is moving in the $+\hat{z}$ axis direction. P_t denotes the transverse momentum. The first

Table I: The unpolarized cross sections of $e^-e^+ \rightarrow e^-e^+\phi$, where ϕ is either the SM Higgs boson H , the CP-even boson h or the CP-odd A . We have taken $\sqrt{S} = 1$ TeV, $m_\phi = 115$ GeV, $g_{hVV} = 0.1$ and $\tilde{g}_{AVV} = 0.1$ for $V = Z$ or γ . (Only one anomalous coupling is taken to be non-zero for each case.) We have imposed the basic cuts of Eq. (4) in order to avoid the divergent collinear behavior of the scattering processes arising from the $\phi\gamma\gamma$ couplings.

process	$\sigma(\text{fb})$	
	$ M_{34} - m_Z < 10 \text{ GeV}$	$ M_{34} - m_Z > 10 \text{ GeV}$
$e^-e^+ \rightarrow e^-e^+H$	0.42	9.0
$e^-e^+ \rightarrow e^-e^+h$ (g_{hZZ})	0.88	8.6
$e^-e^+ \rightarrow e^-e^+h$ ($g_{h\gamma\gamma}$)	0.44	13.9
$e^-e^+ \rightarrow e^-e^+A$ (\tilde{g}_{AZZ})	0.21	0.17
$e^-e^+ \rightarrow e^-e^+A$ ($\tilde{g}_{A\gamma\gamma}$)	0.02	4.22

two cuts are required to avoid collinear divergences in the t -channel process, whereas the third cut is required to avoid the divergence when the s -channel photon goes on-shell when ignoring the electron mass in the helicity amplitude calculations. Furthermore, the requirement on the cosine of the polar angles $|\cos\theta| \leq 0.99$, which corresponds to $172^\circ \geq \theta \geq 8^\circ$, will ensure that the final state leptons fall within the detector coverage at the ILC.

The cross section for $e^-e^+ \rightarrow e^-e^+\phi$ with unpolarized beams and a fixed value of the coupling coefficients is shown in Table I. The SM prediction for the $e^-e^+ \rightarrow ZH \rightarrow e^-e^+H$ process is about 0.4 fb, much smaller than the 9 fb predicted for the t -channel ZZ fusion process at $\sqrt{S} = 1$ TeV. The purpose of this work is to distinguish between the CP-even and CP-odd scalars, and we will concentrate on studying the t -channel process. Table I also shows that the contribution from the $\phi\gamma\gamma$ coupling is potentially larger than the contribution from the anomalous ϕZZ coupling with the same magnitude. This is because the collinear divergences mentioned above only appear in scattering processes with nearly on-shell photon.

Apart from analyzing the usual kinematic distributions, we will also consider the following angular variables which will be shown later to be sensitive to the CP nature of Higgs boson:

$$\begin{aligned}
X_{e^-e^+} &\equiv X \equiv (\hat{p}_3 - \hat{p}_4) \cdot \hat{p}_1 = \cos\theta_3 - \cos\theta_4, \\
Y_{e^-e^+} &\equiv Y \equiv \frac{\hat{p}_3 \cdot (\vec{p}_1 \times \vec{p}_4)}{|\vec{p}_1 \times \vec{p}_4|} - \frac{\hat{p}_4 \cdot (\vec{p}_1 \times \vec{p}_3)}{|\vec{p}_1 \times \vec{p}_3|},
\end{aligned} \tag{5}$$

where the unit vectors $\hat{p}_i = \vec{p}_i/|\vec{p}_i|$. Generally, the experimental analysis of these variables would require particle identification of the outgoing leptons. However, the absolute values of $X_{e^-e^+}$ and $Y_{e^-e^+}$ could also be used with the advantage of not requiring to determine the charge of the outgoing leptons, separating e^+ from e^- in the final state, to discriminate a CP-even from a CP-odd Higgs boson.

B. Comparison of production rates from the $\phi\gamma\gamma$, $\phi Z\gamma$ and ϕZZ couplings in the t -channel process

For the rest of this work we focus our attention on the t -channel process, so that we will require the e^-e^+ invariant mass to be away from the Z mass value:

$$|M_{34} - m_Z| \geq 10 \text{ GeV}. \quad (6)$$

It is understood that the conditions of Eqs. (4) and (6) are being applied to the following analysis. We will refer to these conditions as *basic cuts*.

In Fig. 2 we show the $e^-e^+ \rightarrow e^-e^+h$ production cross section induced by each of the 3 couplings, $g_{h\gamma\gamma}$, $g_{hZ\gamma}$ and g_{hZZ} . Only one coupling is taken to be non-zero for each case. Because of the collinear divergent behavior originated from the photon propagator, the contribution from the $h\gamma\gamma$ coupling is much larger for similar values of the coupling coefficients.

For the case of $e^-e^+ \rightarrow e^-e^+A$ production, the cross section depends directly on the \tilde{g}_{AVV} coupling. We can write down the numerical value of the production cross section as:

$$\begin{aligned} \sigma(A\gamma\gamma) &= 421 \times \tilde{g}_{A\gamma\gamma}^2 \text{ (fb)}, \\ \sigma(AZ\gamma) &= 145 \times \tilde{g}_{AZ\gamma}^2 \text{ (fb)}, \\ \sigma(AZZ) &= 21.4 \times \tilde{g}_{AZZ}^2 \text{ (fb)}. \end{aligned} \quad (7)$$

In general, it is not possible to predict the relative sizes of the anomalous coupling coefficients without knowing the underlying theory. In case that the underlying physics induce all three effective couplings with similar size, the $\phi\gamma\gamma$ coupling will produce the biggest effect on the t -channel production rate of Higgs boson. Thus, hereafter, we will assume that the effect of this coupling indeed dominates the Higgs boson production rate and we shall focus our attention on the effect of this coupling to various kinematic distributions of the CP-even and CP-odd Higgs boson signal events.

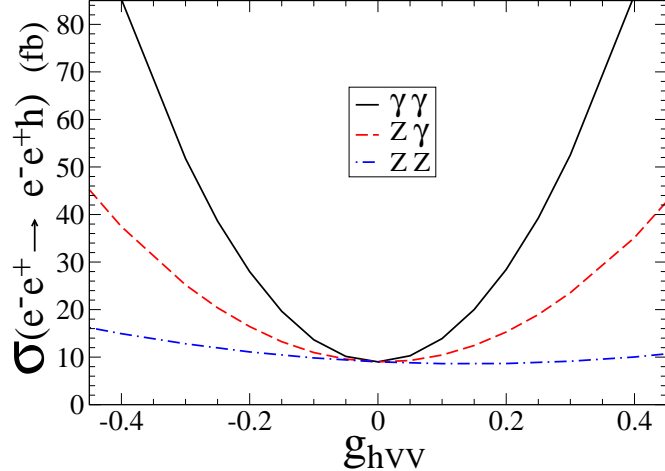


Figure 2: The unpolarized $e^-e^+ \rightarrow e^-e^+h$ production cross section for different values of the 3 CP-even coupling coefficients: $g_{h\gamma\gamma}$, $g_{hZ\gamma}$ and g_{hZZ} . The *basic cuts*, Eqs. (4) and (6), have been applied, and only one anomalous coupling is taken to be non-zero for each case.

C. Unpolarized beams

After imposing the *basic cuts*, cf. Eqs. (4) and (6), we show in Fig. 3 a few kinematic distributions which are useful for determining the CP property of the Higgs boson. They are the distributions of the transverse momentum and energy of the Higgs boson and lepton, and the invariant mass of the two final state leptons.

The results shown in Fig. 3 can be understood as follows. The small tail in the low mass region of the lepton pair invariant mass plot suggests that the production rate is dominated by the ZZ and/or $\gamma\gamma$ fusion processes, and the s -channel process is not as important as the t -channel process in high energy collision with center-of-mass energy around 1 TeV. The SM Higgs boson production is through the dimension-4 HZZ interaction only. While the CP-even Higgs boson h could be produced through either the dimension-4 hZZ or the anomalous $h\gamma\gamma$ interaction, the CP-odd Higgs boson could only be produced through the $A\gamma\gamma$ interaction. Because of the propagator of the Z -boson in the ZZ fusion process, the typical transverse momentum of the final state lepton after emitting the Z boson in the ZZ fusion process is about half of the Z boson mass. In case of the production of the CP-odd Higgs boson via $\gamma\gamma$ fusion, the final state lepton typically has a smaller transverse momentum, cf. Fig. 3(c), due to the collinear enhancement in the emission of an effective

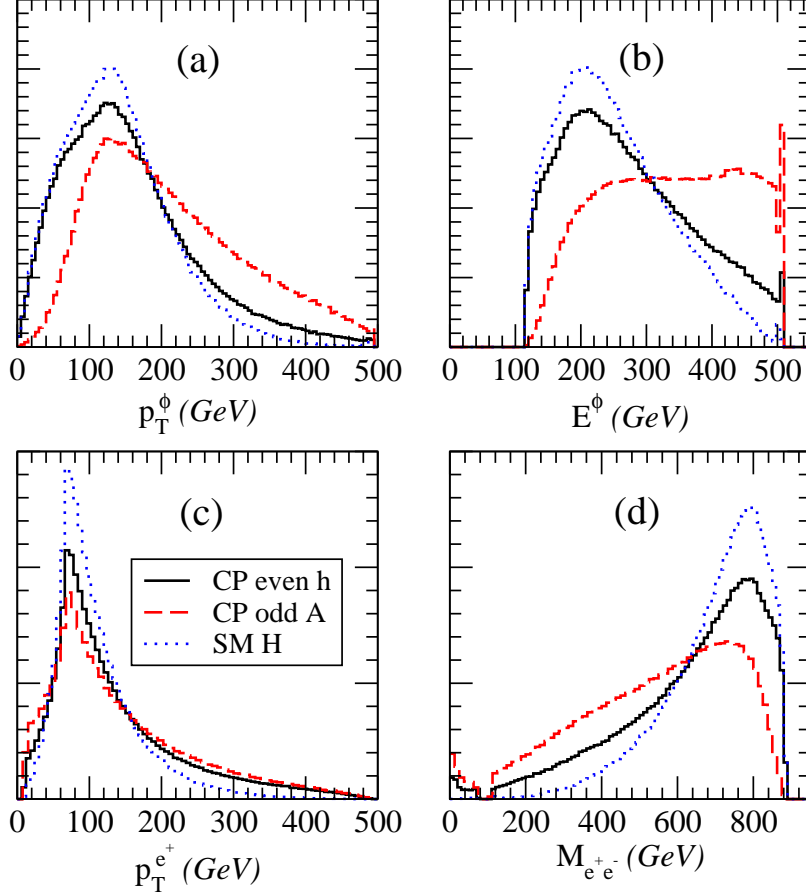


Figure 3: The normalized differential cross sections for the $e^-e^+ \rightarrow e^-e^+\phi$ processes as a function of the corresponding kinematical variable. We show the distributions for the SM H (blue dotted line), the CP-even h (black solid line) and the CP-odd A (red dashed line) Higgs bosons. The values $g_{h\gamma\gamma} = \tilde{g}_{A\gamma\gamma} = 0.1$ have been used. The *basic cuts* (Eqs. (4) and (6)) have been applied.

photon from the lepton. Since the effective photon is transversely polarized, the lepton after emitting the effective photon in the $\gamma\gamma$ fusion process can have a large angle relative to the beam axis, and yields a smaller magnitude in the absolute value of its rapidity. In contrast, after emitting a longitudinal (virtual) Z boson, the lepton prefers to move along the forward direction which is obvious from the consideration of helicity conservation. The net effect of the collinear enhancement and the transverse polarization of the emitted effective photon to the lepton rapidity distribution can be seen in Fig. 4(a), which shows the rapidity distribution of the final state electron with the choice of the incoming electron in the $+\hat{z}$ direction. The distribution of the final state positron is not shown because it has the same

shape as the electron's but in the negative rapidity direction. As compared to the lepton rapidity distribution predicted by the SM, the one predicted for the CP-odd Higgs boson shows a flatter distribution. The result for the CP-even non-SM Higgs boson h lies between the above two curves. In Fig. 4(b), we also show the distribution of the rapidity difference, in its absolute value, between the two final state leptons in the Higgs boson events. By taking only the absolute value of the rapidity difference between the two charged leptons, we eliminate the requirement of identifying the electrical charge of the two outgoing leptons, i.e., separating e^+ from e^- , which could be challenging for leptons with large rapidity (in magnitude). For completeness, we also show in Fig. 4(c) the distribution of the lepton rapidity difference without taking its absolute values (for the case that the electrical charge of the lepton is identified). Due to the collinear enhancement discussed above, very little event rate falls into the negative region.

Next, let us discuss the kinematic distributions of the Higgs bosons. As shown in Figs. 3(a) and (b), the energy of the CP-odd Higgs boson is typically higher than that of the SM Higgs boson because the invariant mass of the final state lepton pairs in the CP-odd Higgs signal events is lower than that in the SM Higgs signal events, cf. Fig. 3(d), which is due to the lower transverse momentum that the final state leptons can have in the CP-odd Higgs events. Furthermore, due to the transversity of the emitted effective photon in the $\gamma\gamma$ fusion process, the possibility for producing two energetic leptons from $\gamma\gamma$ fusion process is small, therefore the energy distribution of the CP-odd Higgs boson drops very fast in the small energy region, cf. Fig. 3(b). The same reasoning also explains the transverse momentum distribution of the Higgs boson in Fig. 3(a). In all cases, the maximal allowed value for the energy of the Higgs boson E^ϕ is constrained by the center-of-mass energy (\sqrt{S}) of the collider and the masses of final state particles, it is

$$E_{\max}^\phi = \frac{\sqrt{S}}{2} - \frac{(m_{e^+} + m_{e^-})^2 - m_\phi^2}{2\sqrt{S}} \sim 507 \text{ GeV}, \quad (8)$$

as can be deduced from the three-body phase space.

We note that in the above kinematic distributions, the CP-odd Higgs boson differs from the CP-even Higgs boson, but the CP-even Higgs boson has similar distributions as the SM Higgs boson. To separate the CP-even Higgs boson from the SM Higgs boson background, one could make use of the rapidity distributions of the final state leptons, as shown in Fig. 4.

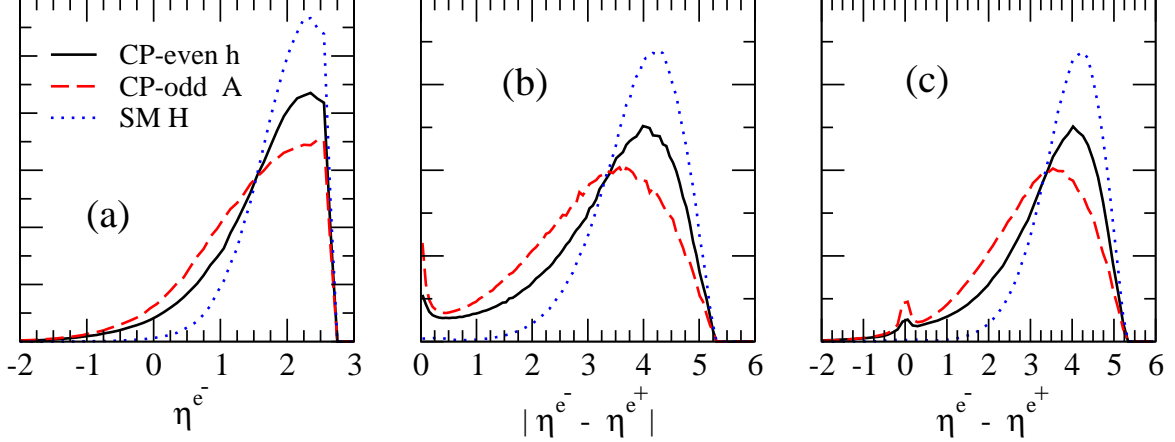


Figure 4: The normalized differential cross section for the $e^-e^+ \rightarrow e^-e^+\phi$ process as a function of the rapidity (difference). We show the distributions for the SM H (blue dotted line), the CP-even h (black solid line) and the CP-odd A (red dashed line) Higgs bosons. The values $g_{h\gamma\gamma} = \tilde{g}_{A\gamma\gamma} = 0.1$ have been used, and the *basic cuts* have been applied.

Table II: The unpolarized cross sections of $e^-e^+ \rightarrow e^-e^+\phi$, where ϕ is either the SM Higgs boson H , the CP-even boson h or the CP-odd A . We have taken $m_\phi = 115$ GeV and considered the following cases: $g_{h\gamma\gamma} = \pm 0.1$ and $\tilde{g}_{A\gamma\gamma} = 0.1$. The kinematic cuts listed in each column are applied sequentially.

process	(fb)	(fb)	(fb)
	<i>basic cuts</i>	$ \eta_{e^-} - \eta_{e^+} \leq 3$ GeV	$ \eta_{e^-} - \eta_{e^+} \leq 2$ GeV
$e^-e^+ \rightarrow e^-e^+H$	9.0	1.09	0.17
$e^-e^+ \rightarrow e^-e^+h$ ($g_{h\gamma\gamma} = 0.1$)	13.9	3.50	1.42
$e^-e^+ \rightarrow e^-e^+h$ ($g_{h\gamma\gamma} = -0.1$)	13.7	3.30	1.28
$e^-e^+ \rightarrow e^-e^+A$ ($\tilde{g}_{A\gamma\gamma} = 0.1$)	4.22	1.91	0.91

Since the CP-even Higgs boson h can be produced either from ZZ or $\gamma\gamma$ fusion process, the electron rapidity distribution lies in between the SM Higgs boson and CP-odd Higgs boson. Based on the different shapes in the rapidity distributions of H , h and A , cf. Fig. 4, we can impose further cuts to reduce the SM rate (which is referred below as the “background rate”). In Table II we show the cross sections after demanding the rapidity difference between the two leptons to be smaller than 3 and 2, separately. The former cut, $|\eta_{e^-} - \eta_{e^+}| < 3$,

increases the signal-to-background ratio by about a factor 2 while keeping about 25% of the signal rate for the CP-even Higgs boson for both positive and negative $g_{h\gamma\gamma}$. For the CP-odd Higgs boson, this cut increases the signal-to-background ratio by about a factor of 3.7 while keeping about 45% of the signal rate. That more CP-odd Higgs boson events survive this cut is due to the different electron rapidity distributions as discussed above. As shown in Fig. 4(b), it would be possible to make a substantial reduction (by an order of magnitude) of the SM rate by imposing a lower rapidity difference cut. We observe, nevertheless, that for the stringent cut ($|\eta_{e^-} - \eta_{e^+}| < 2$) with couplings $g_{\phi\gamma\gamma}$ and $\tilde{g}_{\phi\gamma\gamma}$ of order 0.1, only a small cross section of about less than 1 fb may be left. This may make it difficult to observe any events in a more realistic analysis. We therefore choose not to use this stronger cut. For the remainder of this work, in addition to the *basic cuts* we will apply the following cut ²:

$$|\eta_{e^-} - \eta_{e^+}| \leq 3. \tag{9}$$

But it is worth mentioning that with a high luminosity in the upgraded ILC, one could use a tight cut to achieve a better significance.

In Fig. 5, we present a few kinematic distributions after imposing the lepton rapidity difference cut, cf. Eq. (9), together with the *basic cuts*. First of all, we note that the typical invariant mass of the lepton pair becomes smaller because the two leptons have a smaller rapidity separation. Furthermore, the SM Higgs boson rate is suppressed enough that the CP-odd Higgs boson rate becomes comparable to the SM rate. From the conservation of total energy, a smaller $m_{e^-e^+}$ implies a larger energy E_ϕ (and transverse momentum p_{T_ϕ}) of the Higgs boson which is evident in Fig. 5. Again, the $m_{e^-e^+}$ distribution of the CP-even Higgs boson h is similar to the CP-odd Higgs boson A in the small invariant mass $m_{e^-e^+}$ region while similar to the SM Higgs boson H in the large invariant mass $m_{e^-e^+}$ region. However, the detailed distribution depends on the interference pattern generated by the inclusion of the dimension-6 $h\gamma\gamma$ operator. Clearly, the difference in the above mentioned kinematical distributions of the lepton pair and Higgs boson originates from different spin correlations in the scattering amplitudes for producing the three different Higgs bosons. To further investigate their difference, we also show in Fig. 5 the distributions of $\cos(\theta_{e^-} - \theta_{e^+})$

² Notice that the cuts imposed in this work do not require identifying the electric charge of the leptons, i.e., separating e^+ from e^- .

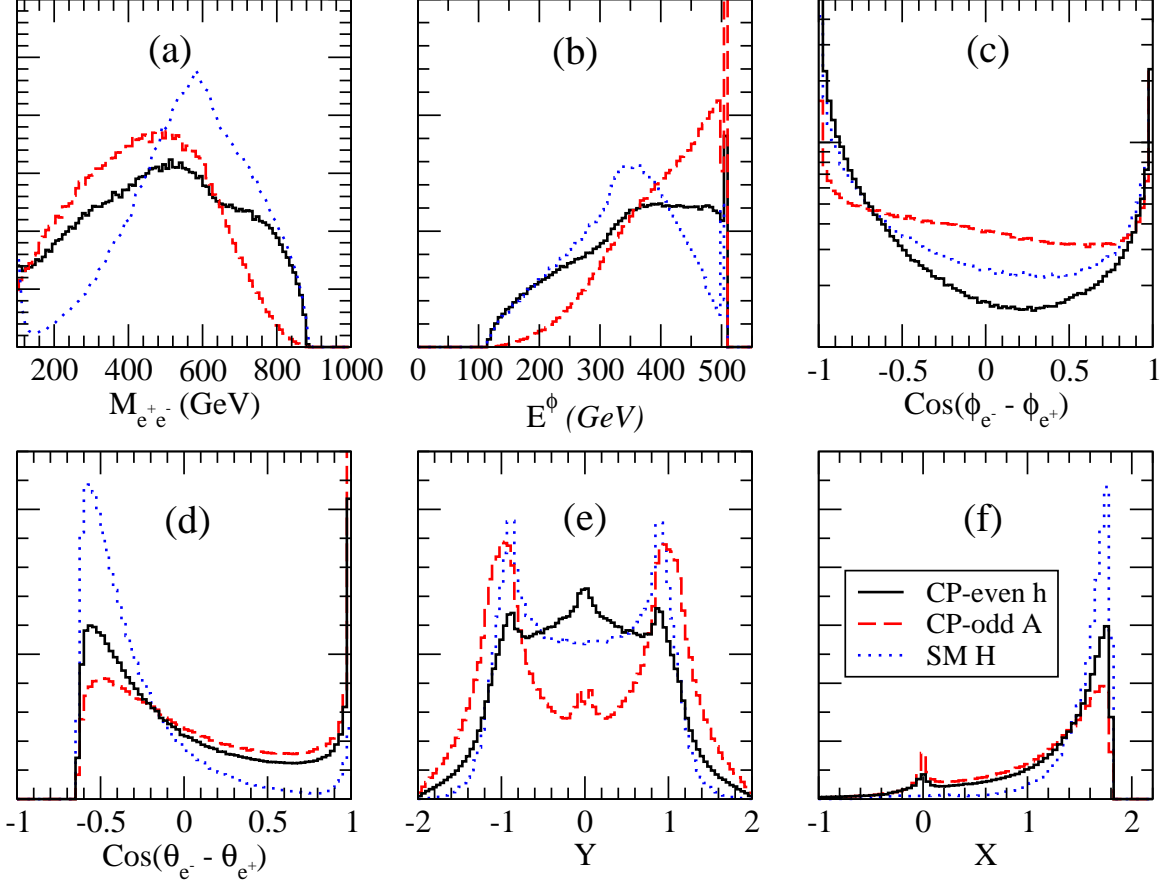


Figure 5: The normalized differential cross sections for the unpolarized $e^-e^+ \rightarrow e^-e^+\phi$ processes as a function of the corresponding kinematical variable. We show the distributions for the SM H (blue dotted line), the CP-even h (black solid line) and the CP-odd A (red dashed line) Higgs bosons. The values $g_{h\gamma\gamma} = \tilde{g}_{A\gamma\gamma} = 0.1$ have been used. The *basic cuts* and the lepton rapidity difference cut, cf. Eq. (9), have been applied.

and $\cos(\phi_{e^-} - \phi_{e^+})$, where θ_i and ϕ_i are the polar and azimuthal angles of the lepton i in the final state, and the two new observables $X_{e^-e^+}$ and $Y_{e^-e^+}$, cf. Eq. (5). The cause of the difference in the distributions of the above physical observables can be better understood when we study the case of polarized beams which will be discussed in the next section.

Since the polarization of the incoming electron and positron beams would be possible at the ILC, it is worth analyzing this possibility. Below we will show that polarized beams are indeed useful for distinguishing a CP-even from a CP-odd Higgs boson.

Table III: Cross section for $e_{\lambda_1}^- e_{\lambda_2}^+ \rightarrow e^- e^+ \phi$ when the initial state leptons are polarized. L and R stand for a left-handed or right-handed polarized lepton beam. We have taken $m_\phi = 115 \text{ GeV}$, $g_{h\gamma\gamma} = 0.1$ and $\tilde{g}_{A\gamma\gamma} = 0.1$.

$\sigma(fb)$	$e_{\lambda_1}^- e_{\lambda_2}^+ \rightarrow e^- e^+ H$				$e_{\lambda_1}^- e_{\lambda_2}^+ \rightarrow e^- e^+ h$				$e_{\lambda_1}^- e_{\lambda_2}^+ \rightarrow e^- e^+ A$			
	LL	LR	RL	RR	LL	LR	RL	RR	LL	LR	RL	RR
<i>basic cuts</i>	8.65	13.17	5.54	8.65	17.16	13.85	7.47	17.16	4.66	3.77	3.77	4.66
with $ \eta_{e^-} - \eta_{e^+} \leq 3$	1.06	1.57	0.67	1.06	4.93	2.33	1.85	4.93	2.21	1.61	1.61	2.21

D. Polarized beams

Let us analyze to what extent the polarization of the collider beams could help us to discriminate between CP eigenstates of Higgs bosons. For simplicity, we assume a 100% degree of polarization. Needless to say that in practice the beam polarization will be only partially longitudinal or partially transverse. Using the rapidity cuts given in Eq. (9) we calculated the rates for the $e_{\lambda_1}^- e_{\lambda_2}^+ \rightarrow e^- e^+ \phi$ (with $\lambda_1, \lambda_2 = L$ or R) processes, which are shown in Table III for all the possible polarization states of the initial leptons. The rates shown in the first row are with the *basic cuts* only, and the rates in the second row are with the additional cut on the lepton rapidity difference, cf. Eq. (9). Since we assume CP is conserved in this study, the production rate of $e_R^- e_R^+$ is the same as the $e_L^- e_L^+$ rate.

For the sake of illustration we will present below the kinematic distributions for left-left and left-right handed polarized beams, i.e. $e_L^- e_L^+ \rightarrow e^- e^+ \phi$ and $e_L^- e_R^+ \rightarrow e^- e^+ \phi$, denoted as LL and LR , respectively.

1. Left-left handed polarized beams

Fig. 6 shows various kinematic distributions for $e_L^- e_L^+ \rightarrow e^- e^+ \phi$ when left-left handed polarized beams are used, in which both the *basic cuts* and the lepton rapidity difference cut, cf. Eq. (9), have been imposed. It is evident from the figure that the use of polarized beams enhances the differences between some distributions, like $\cos(\theta_{e^-} - \theta_{e^+})$ and $Y_{e^- e^+}$ distributions, cf. Eq. (5). We note that for this polarization state of the collider beams there is no s -channel contribution to the production process. The SM Higgs boson H is

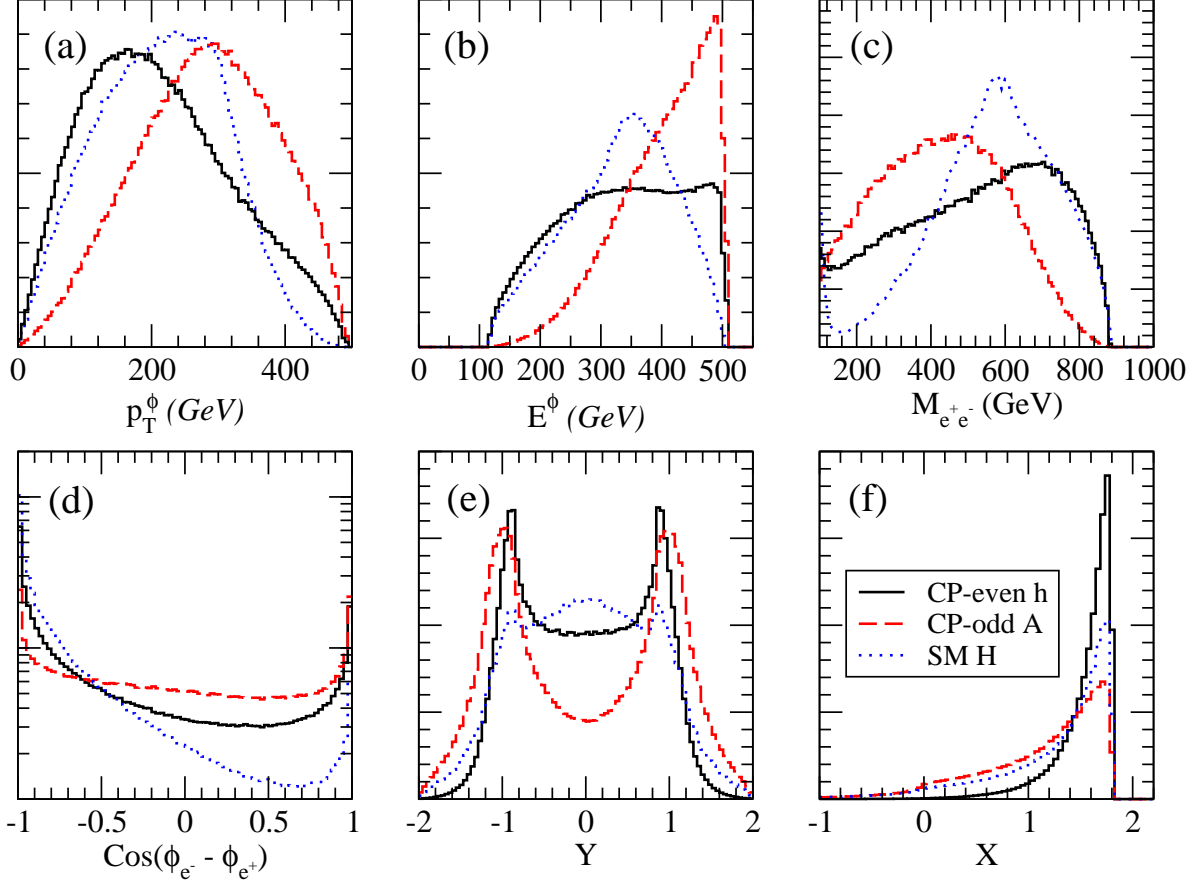


Figure 6: Same as Fig. 5 for left-left polarized beams.

produced from ZZ fusion and the CP-odd Higgs boson A is produced from $\gamma\gamma$ fusion, while the CP-even Higgs boson h can be produced via both ZZ and $\gamma\gamma$ fusion processes. Through a simple algebra, one can show that

$$Y_{e^-e^+} \propto \sin \theta_{e^-} \sin \theta_{e^+} [\cos(\phi_{e^-} + \phi_{e^+}) - \cos(\phi_{e^-} - \phi_{e^+})],$$

therefore, $Y_{e^-e^+}$ and $\cos(\phi_{e^-} - \phi_{e^+})$ provide almost the same information. To investigate the different shapes in the $\cos(\phi_{e^-} - \phi_{e^+})$ and $Y_{e^-e^+}$ distributions between h and H productions, we show in Fig. (7) the distributions of $\cos(\theta_{e^-} - \theta_{e^+})$ and $Y_{e^-e^+}$ after switching off the hZZ interaction in the h production, namely, only the $h\gamma\gamma$ interaction is included in this comparison. It is clear that due to the different CP property of h and A bosons, the distributions of $Y_{e^-e^+}$ are very different for h and A bosons, cf. Fig. 7(b), while the distribution of $\cos(\theta_{e^-} - \theta_{e^+})$ is almost the same for h and A bosons, cf. Fig. 7(a). Hence, we conclude that the azimuthal angle distributions are more sensitive to the CP property of

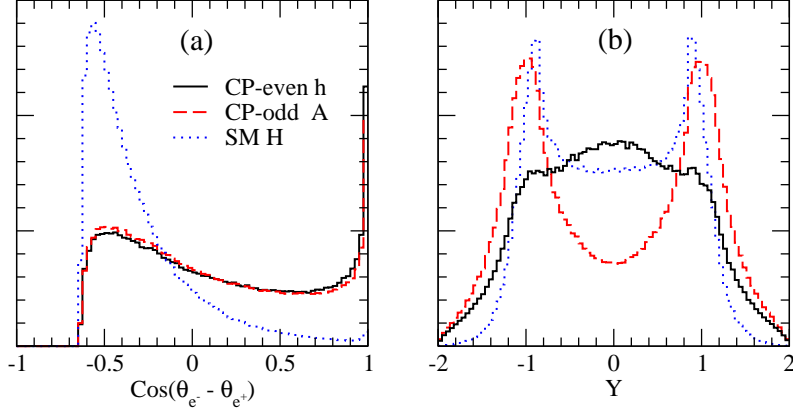


Figure 7: Distributions of $\cos(\theta_{e^-} - \theta_{e^+})$ and $Y_{e^-e^+}$ after switching off the hZZ interaction in the h production, namely, only the $h\gamma\gamma$ interaction is included in this comparison.

the Higgs bosons. Particularly, in the $Y_{e^-e^+}$ distribution, a dip occurs around $Y = 0$ for the CP-odd A boson production. In contrast, the rate is enhanced at $Y = 0$ for the CP-even h boson production. Needless to say that after turning back on the hZZ interaction, the distributions of the h boson production are also affected by the interference effect between the hZZ and $h\gamma\gamma$ interactions which results in the actual distributions shown in Fig. 6. Similar conclusion also holds for the $\cos(\phi_{e^-} - \phi_{e^+})$ distributions.

2. Left-right handed polarized beams

Next, we consider the case that the electron beam is left-handedly polarized while the positron beam is right-handedly polarized. For this polarization state of the collider beams, both s - and t -channel processes contribute to the production of Higgs boson. In Fig. 8, we show the similar kinematic distributions discussed above for comparison. One distinct feature in this set of distributions is that there are enhancement rates (spikes) when the energy E_ϕ and transverse momentum p_{T_ϕ} of the Higgs boson are near 500 GeV, $\cos(\theta_{e^-} - \theta_{e^+})$ and $\cos(\phi_{e^-} - \phi_{e^+})$ are near 1, and both $X_{e^-e^+}$ and $Y_{e^-e^+}$ are near 0. All of these spikes originate from the s -channel process. In the s -channel production process, the invariant mass of the di-lepton pair can take a small value, *i.e.*, the di-lepton pair is produced from the decay of Z boson or a low invariant mass of virtual photon. Obviously, the enhancement factor is larger for a di-lepton pair produced from a low mass virtual photon than an on-shell Z

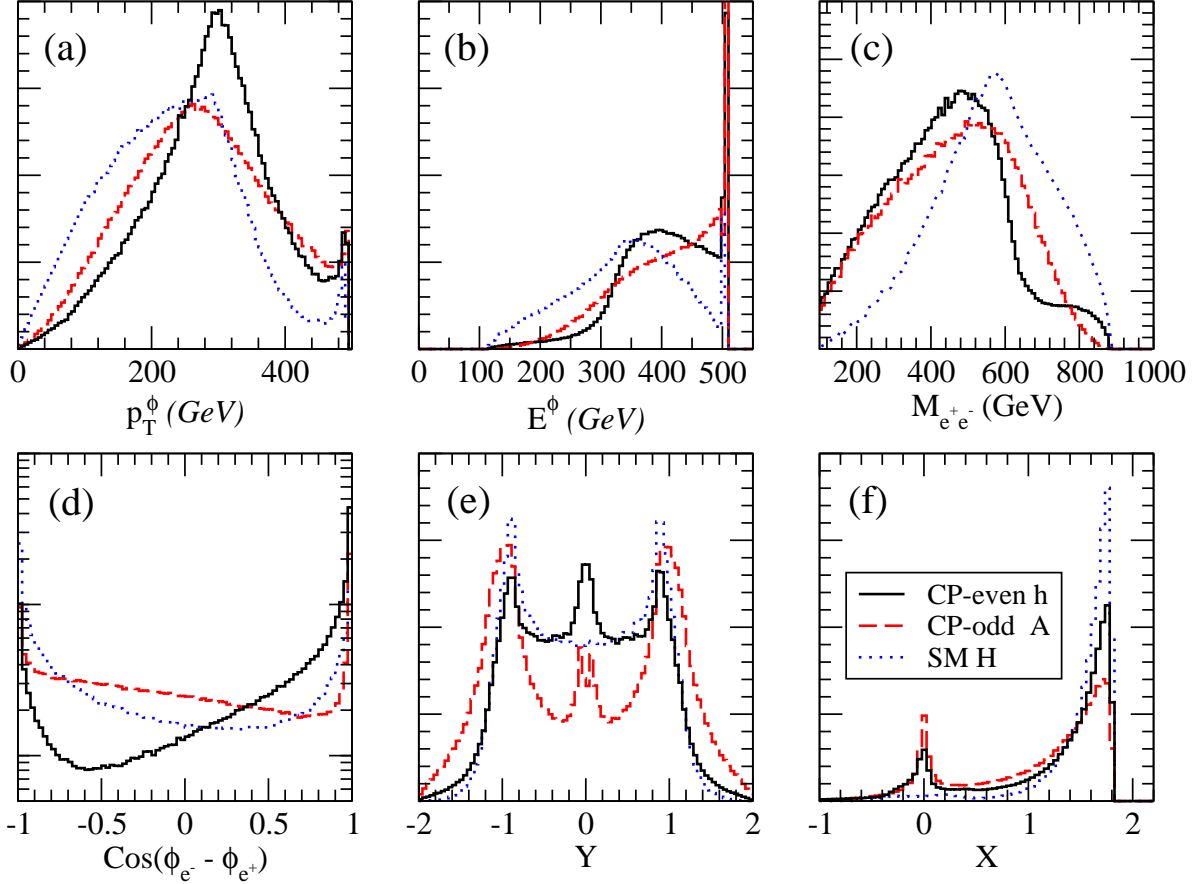


Figure 8: Same as Fig. 5, but for left-right polarized beams.

boson. That explains why, for example, in the $Y_{e^-e^+}$ distribution, both h and A production show a strong peak than the H production in which only the dimension-4 HZZ coupling is considered.

IV. CONCLUSIONS

We study the production of Higgs boson (ϕ) via the $e^-e^+ \rightarrow e^-e^+\phi$ process at a future International Linear Collider (ILC) with $\sqrt{S} = 1$ TeV. At this energy the Standard Model ZZ -fusion rate dominates over the associated ZH production rate. Here, we consider a class of theory models based on the effective ϕVV (with $V = Z, \gamma$) couplings generated by dimension-6 operators. We also show how to use the kinematical distributions of the final state leptons to discriminate the CP-even and CP-odd Higgs bosons produced at the ILC, when the $\phi\gamma\gamma$ coupling dominates the Higgs boson production rate. Assuming the Higgs

boson is identified, we have found that the kinematical distributions (and correlations) of the final state e^-e^+ pair can be used to test the CP nature of the Higgs boson. In particular, we have found that requiring the absolute value of their rapidity difference to be within 3 can greatly reduce the SM rate so that the contributions from anomalous couplings are relatively enhanced and it becomes easier to use $\phi\gamma\gamma$ couplings to determine the CP property of Higgs boson. One advantage of these cuts is that it is not necessary to determine the electric charge of the final state e^-e^+ pair. (Particle identification could be challenging for leptons with large rapidity values (in magnitude).) Furthermore, we define two kinematical variables $X_{e^-e^+}$ and $Y_{e^-e^+}$. The shapes of these distributions for a CP-even Higgs boson are different from those for a CP-odd Higgs boson. To distinguish a CP-odd Higgs boson from a CP-even Higgs boson produced via $e^-e^+ \rightarrow e^-e^+\phi$ process at a 1 TeV ILC, it is most effective to use a left-handedly polarized electron beam colliding a left-handedly polarized positron beam, and the observable with the biggest discriminating power is the $Y_{e^-e^+}$ distribution, as defined in Eq. (5).

Acknowledgments

We thank T. Tait and A. Belyaev for helpful discussions. The work of Q.-H.C is supported by the U.S. Department of Energy under grant No. DE-FG03-94ER40837. G.T.V acknowledges support from SNI and SEP-PROMEP. F. Larios acknowledges support from Conacyt and the Fulbright-Garcia Robles fellowship. The work of C.-P. Y. was supported in part by the U. S. National Science Foundation under award PHY-0244919.

-
- [1] M. Carena and H. E. Haber, *Prog. Part. Nucl. Phys.* **50**, 63 (2003), hep-ph/0208209.
- [2] M. C. Gonzalez-Garcia, S. M. Lietti, and S. F. Novaes, *Phys. Rev.* **D59**, 075008 (1999), hep-ph/9811373.
- [3] R. P. Kauffman and S. V. Desai, *Phys. Rev.* **D59**, 057504 (1999), hep-ph/9808286.
- [4] T. Plehn, D. L. Rainwater, and D. Zeppenfeld, *Phys. Rev. Lett.* **88**, 051801 (2002), hep-ph/0105325.
- [5] B. Field, *Phys. Rev.* **D66**, 114007 (2002), hep-ph/0208262.
- [6] S. Y. Choi, D. J. Miller, M. M. Muhlleitner, and P. M. Zerwas, *Phys. Lett.* **B553**, 61 (2003), hep-ph/0210077.
- [7] T. Figy and D. Zeppenfeld, *Phys. Lett.* **B591**, 297 (2004), hep-ph/0403297.
- [8] V. D. Barger, K.-m. Cheung, A. Djouadi, B. A. Kniehl, and P. M. Zerwas, *Phys. Rev.* **D49**, 79 (1994), hep-ph/9306270.
- [9] W. Kilian, M. Kramer, and P. M. Zerwas, *Phys. Lett.* **B381**, 243 (1996), hep-ph/9603409.
- [10] P. Minkowski, *Int. J. Mod. Phys.* **13**, 2255 (1998).
- [11] K. Hagiwara, S. Ishihara, J. Kamoshita, and B. A. Kniehl, *Eur. Phys. J.* **C14**, 457 (2000), hep-ph/0002043.
- [12] B. Grzadkowski, J. F. Gunion, and J. Pliszka, *Nucl. Phys.* **B583**, 49 (2000), hep-ph/0003091.
- [13] B. Grzadkowski and J. Pliszka, *Phys. Rev.* **D63**, 115010 (2001), hep-ph/0012110.
- [14] J. F. Gunion, H. E. Haber, and R. Van Kooten, *Linear Collider Physics in the new Milenium*, (edited by K. Fuji, D. Miller and A. Soni) (2003), hep-ph/0301023.
- [15] V. Barger, T. Han, P. Langacker, B. McElrath, and P. Zerwas, *Phys. Rev.* **D67**, 115001 (2003), hep-ph/0301097.
- [16] K. Desch, A. Imhof, Z. Was, and M. Worek, *Phys. Lett.* **B579**, 157 (2004), hep-ph/0307331.
- [17] M. T. Dova and S. Ferrari, *Phys. Lett.* **B605**, 376 (2005), hep-ph/0406313.
- [18] A. Rouge, *Phys. Lett.* **B619**, 43 (2005), hep-ex/0505014.
- [19] J. R. Ellis, J. S. Lee, and A. Pilaftsis, *Phys. Rev.* **D72**, 095006 (2005), hep-ph/0507046.
- [20] S. S. Biswal, R. M. Godbole, R. K. Singh, and D. Choudhury, *Phys. Rev.* **D73**, 035001 (2006), hep-ph/0509070.

- [21] T. Han and J. Jiang, Phys. Rev. **D63**, 096007 (2001), hep-ph/0011271.
- [22] B. Grzadkowski and J. F. Gunion, Phys. Lett. **B294**, 361 (1992), hep-ph/9206262.
- [23] G. J. Gounaris and G. P. Tsirigoti, Phys. Rev. **D56**, 3030 (1997), hep-ph/9703446.
- [24] J. R. Ellis, J. S. Lee, and A. Pilaftsis, Nucl. Phys. **B718**, 247 (2005), hep-ph/0411379.
- [25] P. Niezurawski, A. F. Zarnecki, and M. Krawczyk, Acta Phys. Polon. **B36**, 833 (2005), hep-ph/0410291.
- [26] J. F. Gunion, T. Han, and R. Sobey, Phys. Lett. **B429**, 79 (1998), hep-ph/9801317.
- [27] S. Weinberg, Physica **A96**, 327 (1979).
- [28] H. Georgi, Nucl. Phys. **B361**, 339 (1991).
- [29] W. Buchmuller and D. Wyler, Nucl. Phys. **B268**, 621 (1986).
- [30] C. Arzt, M. B. Einhorn, and J. Wudka, Nucl. Phys. **B433**, 41 (1995), hep-ph/9405214.
- [31] K. Hagiwara, R. Szalapski, and D. Zeppenfeld, Phys. Lett. **B318**, 155 (1993), hep-ph/9308347.
- [32] K. Hagiwara and D. Zeppenfeld, Nucl. Phys. **B274**, 1 (1986).
- [33] D. O. Carlson, Physics of single-top quark production at hadron colliders (PhD thesis), hep-ph/9508278.

Appendix A: HELICITY AMPLITUDES FOR $e^-e^+ \rightarrow e^-e^+\phi$

In this appendix we outline the calculation of the helicity amplitudes for $e^-e^+ \rightarrow e^-e^+\phi$. We use the method of Ref. [32, 33], which breaks down the four-dimensional Dirac algebra into an equivalent two-dimensional one. In the Weyl basis, Dirac spinors have the form

$$\begin{pmatrix} \psi_+ \\ \psi_- \end{pmatrix}, \quad (\text{A1})$$

where

$$\psi_\pm = \begin{cases} u_\pm^{(\lambda=1)} = \omega_\pm \chi_{1/2} \\ u_\pm^{(\lambda=-)} = \omega_\mp \chi_{-1/2} \end{cases} \quad (\text{A2})$$

for fermions and

$$\psi_\pm = \begin{cases} v_\pm^{(\lambda=1)} = \pm \omega_\mp \chi_{-1/2} \\ v_\pm^{(\lambda=-)} = \mp \omega_\pm \chi_{1/2} \end{cases} \quad (\text{A3})$$

for antifermions. $\omega_\pm = \sqrt{E \pm |\vec{p}|}$ and $\chi_{\lambda/2}$ stands for the eigenvectors of the helicity operator $\hat{p} \cdot \vec{\sigma}$ with eigenvalue $\lambda = 1$ for spin-up fermions and $\lambda = -1$ for spin-down fermions:

$$\chi_{1/2} = \begin{pmatrix} \cos \theta/2 \\ e^{i\phi} \sin \theta/2 \end{pmatrix}, \quad \chi_{-1/2} = \begin{pmatrix} -e^{i\phi} \sin \theta/2 \\ \cos \theta/2 \end{pmatrix}. \quad (\text{A4})$$

We will use the shorthand notation $|p_i \pm\rangle$ for $\chi_{\pm 1/2}$. In this basis, the Dirac matrices have the form

$$\gamma^0 = \begin{pmatrix} 0 & 1 \\ 1 & 0 \end{pmatrix}, \quad \gamma^j = \begin{pmatrix} 0 & -\sigma_j \\ \sigma_j & 0 \end{pmatrix}, \quad \gamma^5 = \begin{pmatrix} 1 & 0 \\ 0 & -1 \end{pmatrix}, \quad (\text{A5})$$

where σ_j are the 2×2 Pauli matrices. We can write

$$\not{p} = \begin{pmatrix} 0 & p_0 + \vec{\sigma} \cdot \vec{p} \\ p_0 - \vec{\sigma} \cdot \vec{p} & 0 \end{pmatrix} \equiv \begin{pmatrix} 0 & \not{p}_+ \\ \not{p}_- & 0 \end{pmatrix}, \quad (\text{A6})$$

where $\gamma_\pm^\mu = (1, \mp \vec{\sigma})$. Let us denote the helicity amplitudes by $\mathcal{M}(\lambda_{e_1^-}, \lambda_{e_2^+}, \lambda_{e_3^-}, \lambda_{e_4^+})$, where λ_i represents the helicity of the particle i . The convention for the momenta of the external particles is given in Eq. (3). After a straightforward calculation, the following helicity amplitudes for $e^-e^+ \rightarrow e^-e^+\phi$ are obtained.

1. SM Higgs boson

The SM Higgs boson can be produced through the Higgstrahlung or ZZ -fusion process, as shown in Fig. 9. The former is s -channel like but the latter is t -channel like. The helicity amplitudes $\mathcal{M}_{SM}^{HZZ}(\lambda_{e_1^-}, \lambda_{e_2^+}, \lambda_{e_3^-}, \lambda_{e_4^+})$ for the SM Higgs boson production via $e^-(p_1, \lambda_{e_1^-})e^+(p_2, \lambda_{e_2^+}) \rightarrow e^-(p_3, \lambda_{e_3^-})e^+(p_4, \lambda_{e_4^+})H(p_5)$ are listed as follows:

$$\mathcal{M}_{SM}^{HZZ}(++++) = C_{fac} \frac{2 g_{HZZ} e_L^Z e_R^Z}{(p_k^2 - m_Z^2)(p_q^2 - m_Z^2)} \langle 1-|2+ \rangle \langle 4+|3- \rangle, \quad (\text{A7})$$

$$\mathcal{M}_{SM}^{HZZ}(----) = C_{fac} \frac{2 g_{HZZ} e_L^Z e_R^Z}{(p_k^2 - m_Z^2)(p_q^2 - m_Z^2)} \langle 1-|4+ \rangle \langle 2+|3- \rangle, \quad (\text{A8})$$

$$\mathcal{M}_{SM}^{HZZ}(-++-) = C_{fac} \frac{2 g_{HZZ} e_L^Z e_R^Z}{(p_l^2 - m_Z^2)(p_m^2 - m_Z^2)} \langle 2-|4+ \rangle \langle 3+|1- \rangle, \quad (\text{A9})$$

$$\mathcal{M}_{SM}^{HZZ}(+--+) = C_{fac} \frac{2 g_{HZZ} e_L^Z e_R^Z}{(p_l^2 - m_Z^2)(p_m^2 - m_Z^2)} \langle 2+|4- \rangle \langle 3-|1+ \rangle, \quad (\text{A10})$$

$$\mathcal{M}_{SM}^{HZZ}(-+-+) = C_{fac} \left\{ \frac{2 g_{HZZ} e_L^Z e_R^Z}{(p_k^2 - m_Z^2)(p_q^2 - m_Z^2)} \langle 4+|3- \rangle \langle 1-|2+ \rangle \right. \\ \left. + \frac{2 g_{HZZ} e_R^Z e_L^Z}{(p_l^2 - m_Z^2)(p_m^2 - m_Z^2)} \langle 2-|3+ \rangle \langle 4+|1- \rangle \right\}, \quad (\text{A11})$$

$$\mathcal{M}_{SM}^{HZZ}(+-+-) = C_{fac} \left\{ \frac{2 g_{HZZ} e_L^Z e_R^Z}{(p_k^2 - m_Z^2)(p_q^2 - m_Z^2)} \langle 1+|2- \rangle \langle 4-|3+ \rangle \right. \\ \left. + \frac{2 g_{HZZ} e_L^Z e_R^Z}{(p_l^2 - m_Z^2)(p_m^2 - m_Z^2)} \langle 2-|3+ \rangle \langle 4+|1- \rangle \right\}. \quad (\text{A12})$$

Here,

$$e_L^Z = \frac{1}{c_W} \left(-\frac{1}{2} + s_W^2 \right), \\ e_R^Z = -s_W,$$

and the SM H - Z - Z coupling is

$$g_{HZZ} = \frac{g}{c_W} m_Z,$$

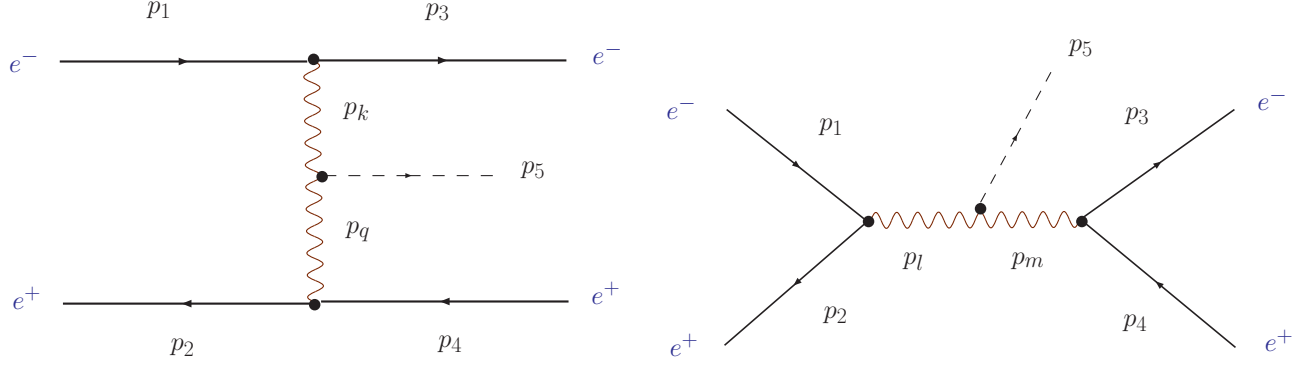


Figure 9: Feynman diagrams for $e^- e^+ \rightarrow e^- e^+ \phi$.

in which $s_W = \sin \theta_W$ and $c_W = \cos \theta_W$ with θ_W being the weak mixing angle. The common factor C_{fac} is defined as

$$C_{fac} = (-ig^2) \sqrt{2E_1} \sqrt{2E_2} \sqrt{2E_3} \sqrt{2E_4},$$

and the momenta of the intermediate state particles are defined as $p_q = p_2 - p_4$, $p_k = p_1 - p_3$, $p_l = p_1 + p_2$, and $p_m = p_3 + p_4$.

2. CP-even Higgs Boson

The CP-even Higgs boson gets both the SM-like contribution and the anomalous contribution,

$$\mathcal{M}_{even} = \mathcal{M}_{SM}^{hZZ} + \sum_{V=\gamma, Z} \mathcal{M}^{hVV}.$$

The SM-like contribution can easily be obtained from Sec. A 1 by replacing the SM Higgs boson (H) with the CP-even Higgs boson (h). The anomalous contributions are listed as follows:

$$\mathcal{M}^{hVV}(++++) = C_{fac} \frac{g_{hVV} e_L^V e_R^V}{p_k^2 p_q^2} \left\{ 2(p_k \cdot p_q) \langle 1+|4- \rangle \langle 2-|3+ \rangle - \langle 1+|\not{p}_{q-}|3+ \rangle \langle 2-|\not{p}_{k+}|4- \rangle \right\}, \quad (\text{A13})$$

$$\mathcal{M}^{hVV}(----) = C_{fac} \frac{g_{hVV} e_L^V e_R^V}{p_k^2 p_q^2} \left\{ 2(p_k \cdot p_q) \langle 1-|4+ \rangle \langle 2+|3- \rangle - \langle 2-|\not{p}_{q+}|1- \rangle \langle 3+|\not{p}_{k-}|4+ \rangle \right\}, \quad (\text{A14})$$

$$\mathcal{M}^{hVV}(-++-) = C_{fac} \frac{g_{hVV} e_L^{\gamma V} e_R^V}{p_l^2 p_m^2} \left\{ 2(p_l \cdot p_m) \langle 2-|4+ \rangle \langle 3+|1- \rangle - \langle 2-|\not{p}_{m+}|1- \rangle \langle 3+|\not{p}_{l-}|4+ \rangle \right\}, \quad (\text{A15})$$

$$\mathcal{M}^{hVV}(+--+) = C_{fac} \frac{g_{hVV} e_L^V e_R^V}{p_l^2 p_m^2} \left\{ 2(p_l \cdot p_m) \langle 2+|4- \rangle \langle 3-|1+ \rangle - \langle 2+|\not{p}_{m-}|1+ \rangle \langle 3-|\not{p}_{l+}|4- \rangle \right\}, \quad (\text{A16})$$

$$\mathcal{M}^{hVV}(-+-+) = C_{fac} \frac{g_{hVV} e_L^V e_R^V}{p_k^2 p_q^2} \left\{ 2(p_k \cdot p_q) \langle 4+|3- \rangle \langle 1-|2+ \rangle - \langle 2-|\not{p}'_{q+}|1- \rangle \langle 3-|\not{p}'_{k+}|4- \rangle \right\} \quad (\text{A17})$$

$$+ C_{fac} \frac{g_{hVV} e_L^V e_R^V}{p_l^2 p_m^2} \left\{ 2(p_l \cdot p_m) \langle 2-|3+ \rangle \langle 4+|1- \rangle - \langle 2-|\not{p}'_{m+}|1- \rangle \langle 3-|\not{p}'_{l+}|4- \rangle \right\}, \quad (\text{A18})$$

$$\mathcal{M}^{hVV}(+-+-) = C_{fac} \frac{g_{hVV} e_L^V e_R^V}{p_k^2 p_q^2} \left\{ 2(p_k \cdot p_q) \langle 1+|2- \rangle \langle 4-|3+ \rangle - \langle 1+|\not{p}'_{q-}|3+ \rangle \langle 2+|\not{p}'_{k-}|4+ \rangle \right\} \\ + C_{fac} \frac{g_{hVV} e_L^V e_R^V}{p_l^2 p_m^2} \left\{ 2(p_l \cdot p_m) \langle 2+|3- \rangle \langle 4-|1+ \rangle - \langle 2+|\not{p}'_{m-}|1+ \rangle \langle 3+|\not{p}'_{l-}|4+ \rangle \right\}.$$

Here,

$$e_L^V = \begin{cases} \frac{1}{c_W} \left(-\frac{1}{2} + s_W^2\right) & V = Z \\ -s_W & V = \gamma \end{cases},$$

$$e_R^V = \begin{cases} \frac{s_W^2}{c_W} & V = Z \\ -s_W & V = \gamma \end{cases},$$

and the anomalous couplings g_{hVV} are related to the coefficients f_i in Eq. (2) by

$$g_{hVV} = -g \frac{s_W^2 m_W}{2\Lambda^2} (f_{BB} + f_{WW}).$$

Again, we have defined $p_q = p_2 - p_4$, $p_k = p_1 - p_3$, $p_l = p_1 + p_2$, and $p_m = p_4 + p_3$.

3. CP-odd Higgs Boson

The CP-odd Higgs boson receives contributions only from the anomalous couplings, i.e.

$$\mathcal{M}_{\text{odd}} = \sum_{V=\gamma, Z} \mathcal{M}^{AVV}.$$

Using the method of Ref. [3], we obtained the following helicity amplitudes:

$$\begin{aligned}
\mathcal{M}^{AVV}(++++) &= C_{fac} \frac{\tilde{g}_{AVV} e_L^V e_R^V}{p_k^2 p_q^2} \left\{ \langle 1+|4-\rangle \langle 2-| \not{p}_{k+} \not{p}_{q-}|3+\rangle - \langle 3-|2+\rangle \langle 4+| \not{p}_{k-} \not{p}_{q+}|1-\rangle \right\}, \\
\mathcal{M}^{AVV}(----) &= C_{fac} \frac{\tilde{g}_{AVV} e_L^V e_R^V}{p_k^2 p_q^2} \left\{ \langle 3+|2-\rangle \langle 4-| \not{p}_{k+} \not{p}_{q-}|1+\rangle - \langle 1-|4+\rangle \langle 2+| \not{p}_{k-} \not{p}_{q+}|3-\rangle \right\}, \\
\mathcal{M}^{AVV}(-++-) &= C_{fac} \frac{\tilde{g}_{AVV} e_L^V e_R^V}{p_l^2 p_m^2} \left\{ \langle 1+|3-\rangle \langle 4-| \not{p}_{l+} \not{p}_{m-}|2+\rangle - \langle 2-|4+\rangle \langle 3+| \not{p}_{l-} \not{p}_{m+}|1-\rangle \right\}, \\
\mathcal{M}^{AVV}+- -+) &= C_{fac} \frac{\tilde{g}_{AVV} e_L^V e_R^V}{p_l^2 p_m^2} \left\{ \langle 2+|4-\rangle \langle 3-| \not{p}_{l+} \not{p}_{m-}|1+\rangle - \langle 1-|3+\rangle \langle 4+| \not{p}_{l-} \not{p}_{m+}|2-\rangle \right\}, \\
\mathcal{M}^{AVV}(-+ -+) &= C_{fac} \frac{\tilde{g}_{AVV} e_L^V e_R^V}{p_k^2 p_q^2} \left\{ \langle 3+|4-\rangle \langle 2-| \not{p}_{k+} \not{p}_{q-}|1+\rangle - \langle 1-|2+\rangle \langle 4+| \not{p}_{k-} \not{p}_{q+}|3-\rangle \right\} \\
&\quad + C_{fac} \frac{\tilde{g}_{AVV} e_L^V e_R^V}{p_l^2 p_m^2} \left\{ \langle 1+|4-\rangle \langle 3-| \not{p}_{l+} \not{p}_{m-}|2+\rangle - \langle 2-|3+\rangle \langle 4+| \not{p}_{l-} \not{p}_{m+}|1-\rangle \right\}, \\
\mathcal{M}^{AVV}+- +-) &= C_{fac} \frac{\tilde{g}_{AVV} e_L^V e_R^V}{p_k^2 p_q^2} \left\{ \langle 1+|2-\rangle \langle 4-| \not{p}_{k+} \not{p}_{q-}|3+\rangle - \langle 3-|4+\rangle \langle 2+| \not{p}_{k-} \not{p}_{q+}|1-\rangle \right\} \\
&\quad + C_{fac} \frac{\tilde{g}_{AVV} e_L^V e_R^V}{p_l^2 p_m^2} \left\{ \langle 2+|3-\rangle \langle 4-| \not{p}_{l+} \not{p}_{m-}|1+\rangle - \langle 1-|4+\rangle \langle 3+| \not{p}_{l-} \not{p}_{m+}|2-\rangle \right\},
\end{aligned}$$

where the anomalous couplings \tilde{g}_{AVV} are related to the coefficients f_i in Eq. (2) by

$$\tilde{g}_{AVV} = -g \frac{s_W^2 m_W}{2\Lambda^2} (f_{BB} + f_{WW}).$$